Monthly Notices of the ROYAL ASTRONOMICAL SOCIETY

MNRAS **498,** 1700–1709 (2020) doi:10.1093/mnras/staa2378
Advance Access publication 2020 August 26

Study of the low-order $\Delta\nu$–$\bar{\rho}$ relation for moderately rotating δ Scuti stars and its impact on their characterization

J. E. Rodríguez-Martín [1,2★] A. García Hernández [1,2★] J. C. Suárez [1,2★] and J. R. Rodón[2]

[1]*Departamento de Física Teórica y del Cosmos, Universdidad de Granada, Campus de Fuentenueva s/n, E-18071 Granada, Spain*
[2]*Instituto de Astrofísica de Andalucía (CSIC), Glorieta de la Astronomía s/n, E-18008 Granada, Spain*

Accepted 2020 August 4. Received 2020 August 4; in original form 2020 April 19

ABSTRACT

The large separation in the low-radial order regime is considered as a highly valuable observable to derive mean densities of δ Scuti stars, due to its independence with rotation. Up to now, theoretical studies of this $\Delta\nu$–$\bar{\rho}$ relation have been limited to 1D non-rotating models and 2D pseudo-evolutionary models. The present work aims at completing this scenario by investigating quantitatively the impact of rotation in this relation on a large grid of 1D asteroseismic models representative of δ Scuti stars. These include rotation effects on both the stellar evolution and the interaction with pulsation. This allowed us to compute the stellar deformation, get the polar and equatorial radii, and correct the stellar mean densities. We found that the new $\Delta\nu$–$\bar{\rho}$ relation for rotating models is compatible with previous works. We explained the dispersion of the points around the linear fits as caused mainly by the distribution of the stellar mass, and partially by the evolutionary stage. The new fit is found to be close to the previous theoretical studies for lower masses (1.3–1.81 $M_\odot$). However, the opposite holds for the observations: For the higher masses (1.81–3 $M_\odot$), the fit is more compatible with the empirical relation. To avoid such discrepancies, we provided new limits to the fit that encompass any possible dependence on mass. We applied these results to characterize the two well-known δ Scuti stars observed by *CoRoT*, HD 174936 and HD 174966, and compared the physical parameters with those of previous works. The inclusion of rotation in the modelling causes a tendency towards greater masses, radii, and luminosities, and lower density values. Comparison between $\Delta\nu$ and *Gaia*'s luminosities also allowed us to constrain the inclination angles and rotational velocities of both stars. The present results pave the way to systematically constrain the angle of inclination (and thereby the actual surface rotation velocity) of δ Scuti stars.

Key words: stars: oscillations – stars: rotation – stars: variables: Scuti.

1 INTRODUCTION

δ Scuti stars are the perfect laboratory to study the effects of rotation. They are stars of late A or early F spectral type, so they are usually rapid rotators (Royer, Zorec & Gómez 2007). Their mass is 1.5–2.5 $M_\odot$ and they belong to the Population I stars (except for the subgroup SX Phe, which belong to the Population II group). They are placed where the main sequence crosses the classic instability strip. The oscillation mechanisms are mainly maintained by the κ mechanism (see, for example, Aerts, Christensen-Dalsgaard & Kurtz 2010). They show radial and non-radial-modes. They are generally low-order p modes with periods from 18 min up to 8 h. Observed amplitudes go from mmag up to the tenths of magnitude (see, for example, Rodríguez & Breger 2001, for a review on their characteristics).

In the last few years, thanks to the technological advances (mainly the space satellites) deeper studies have been done. Uytterhoeven et al. (2011) studied a sample of more than 700 stars with spectral type A–F, observed by the *Kepler* satellite, finding that about 23 per cent of them showed a hybrid γ Dor–δ Scuti behaviour, since they showed p and g modes simultaneously. Murphy et al. (2019) used the parallaxes measured by *Gaia* to obtain precise values of the luminosity of 15 000 stars observed with *Kepler*, finding that not all stars in the classic instability strip are pulsators, only about a 60 per cent. On the other hand, it has been found that the κ mechanism is not the only one responsible for maintaining the oscillations of the δ Scuti star. Coupling between oscillation and convection has also an important role, as shown by Dupret et al. (2005), proving that more modes could be excited and suggesting that the δ Scuti and the γ Dor belong to a same variable star type. Moreover, Xiong et al. (2016) showed that the turbulent motions of convection have to be also taken into account to explain the observed frequency ranges. All this only complicates the interpretation of the oscillation spectra.

In the era of space missions like *MOST* (Matthews 2007), *CoRoT* (Baglin, Michel & Auvergne 2006), *Kepler* (Gilliland et al. 2010), and now *TESS* (Ricker et al. 2009), thanks to ultra-precise photometric time series, periodic patterns could be detected in the p-mode frequency spectra of δ Scuti stars (see e.g. García Hernández et al. 2009, 2013, from now on GH09 and GH13, respectively). These patterns were also predicted theoretically (Ouazzani, Roxburgh & Dupret 2015; Reese et al. 2017) and were found to be compatible with a large separation ($\Delta\nu$; Suárez et al. 2014, from now on S14) since it

★ E-mail: julioeroma@gmail.com (JER-M); agh@ugr.es (AGH); jcsuarez@ugr.es (JCS)

is related to the stellar mean density. This relation was also confirmed for higher rotation rates using 2D models (Reese, Lignières & Rieutord 2008; Mirouh et al. 2019). It was empirically proved using binary systems with a δ Scuti component (García Hernández et al. 2015, from now on GH15). Later on, García Hernández et al. (2017, from now on GH17) showed that it is possible to accurately determine surface gravity of those stars from the $\Delta\nu$–$\bar{\rho}$ relation and a measurement of the parallax. Thanks to all this progress, it has been possible to perform the first multivariable analysis on observed seismic data (Moya et al. 2017), which is an important step towards massive seismic studies of A–F stars.

Despite this progress, the $\Delta\nu$–$\bar{\rho}$ relation is still poorly studied. The previous works mentioned above either used non-rotating (S14) or static 2D equilibrium models (Reese et al. 2008; Mirouh et al. 2019) to derive the relation. Although stellar evolution is mimicked in the latter by considering models with different core hydrogen abundances, this remains a crude approximation compared to what is achieved in 1D stellar evolution codes. Accordingly, the conclusions of these works remain limited. In this context, here we explore the large separation–mean density relation using an extensive grid of rotating models and analyse its behaviour with the physical stellar parameters.

The paper is organized as follows: In Section 2, we explain the methodology of the work, including the characteristics of our asteroseismic models. In Section 3, we revisit the $\Delta\nu$ versus $\bar{\rho}$ relation to study how it is modified by rotation, to what extent, and the implication on asteroseismic determination of stellar magnitudes. In Section 4, we applied the methodology to two δ Scuti stars that were previously studied without including rotation effects. Finally, conclusions are outlined in Section 5.

2 METHODOLOGY

The main objective of this work is to theoretically study the impact of rotation on the relation $\Delta\nu$–$\bar{\rho}$ for A–F stars. To do so, we first need to build a grid of stellar asteroseismic models (stellar structure and oscillations) representative of those stars, similar to the one used by S14 but including rotation during the evolution. With those models, we followed S14's methodology to compute the large separations, which are then paired with the stellar mean density obtained directly from the structure models. We then compare the new $\bar{\rho}$–$\Delta\nu$ relation obtained in this work with those obtained previously without including rotation effects (S14; García Hernández et al. 2015, 2017).

2.1 The equilibrium models

We built a grid composed of more than half a million stellar equilibrium models computed with the CESTAM code (Marques et al. 2013) distributed in 663 evolutionary tracks representative of intermediate-mass stars following in a similar manner as in S14. Models are evolved from the early pre-main sequence (assuming a protostar with a protoplanetary disc) up to the subgiant branch. We constructed the grid by varying three input parameters: mass, metallicity, and initial rotation velocity. The latter is obtained varying the initial rotation period of the protostar and the time (τ) during which the star and the protoplanetary disc are locked. In contrast to S14, we fixed the mixing length convection efficiency to $\alpha = 1.65$ with no overshoot since we consider rotationally induced mixing as prescribed by Zahn (1992) and a further refinement by Mathis & Zahn (2004) for the radiative zones of the stellar interior (more details in Marques et al. 2013).

Table 1. Input parameters for CESTAM. M is the stellar mass (in solar masses), α is the convective efficiency of the mixing length theory, [Fe/H] is the metallicity (in dex), ov is the overshooting parameter, p is the initial rotation period (in days), and τ is the time the protoplanetary disc corrotates with the star (in days).

Input parameter	Range	Step
M	[1.30, 3.00] $M_\odot$	0.05 $M_\odot$
α	1.64	0 fixed
[FeH]	[−0.4, 0.2]	0.1
ov	0.0	fixed
p	[5, 7]	1
τ	5	fixed

In order to ensure a correct computation of the adiabatic oscillations, we imposed a number of shells in which the stellar structure is radially distributed to be above 2000 approximately, as suggested by the ESTA/*CoRoT* working group (Lebreton et al. 2008; Moya & Garrido 2008). Moreover, the stellar models were computed to rotate with $\Omega/\Omega_C \lesssim 0.7$, the vast majority below 0.5. A summary of the input parameters used for CESTAM can be found in Table 1.

2.2 The stellar oscillations

Stellar adiabatic oscillations were computed using the code FILOU (Suárez & Goupil 2008), which computes adiabatic oscillations using a perturbative approximation. It takes into account the stellar distortion due to the centrifugal force in the oscillation frequency computation. Moreover, the code corrects the oscillation frequency for the effects of rotation up to the second order, including near-degeneracy effects (see Suárez, Goupil & Morel 2006, for more details).

Theoretical oscillation modes were computed for each of the equilibrium models of the grid with spherical degree in the range $0 \leq \ell \leq 2$, from a few low-order g modes up to the cut-off frequency, which for these stars is found in the pressure (p) modes domain.

3 THE $\Delta\nu$–$\bar{\rho}$ RELATION

3.1 The large separation

The relation between the large separation and the mean density of δ Scuti stars predicted in S14 held even for rotating models because a significant effect on $\Delta\nu/\sqrt{\bar{\rho}}$ with the distortion of the star is not expected up to 80 per cent of the break-up rotation frequency (Reese et al. 2008). Therefore, a similar relation should be found when rotating models are considered. Following S14, we compute for each model the large separation for each oscillation mode as

$$\Delta\nu_\ell = \nu_{n+1,\ell} - \nu_{n,\ell}, \quad (1)$$

where $\nu_{n,l}$ is the frequency of the mode of radial order n and spherical degree $\ell = 0, 1,$ and $2\,(m = 0)$. To enhance the pattern related with the large separation, we restricted the calculation of $\Delta\nu$ to the range in which δ Scuti stars pulsate, i.e. $2 \leq n \leq 8$. The actual $\Delta\nu_\ell$ for each ℓ is calculated as the median of the individual $\Delta\nu_{n,\ell}$ values. We choose the median instead of the average because it is more stable in case an avoided crossing blurs $\Delta\nu$. In practice, we do not know (by now) which modes are contributing to the observed $\Delta\nu$. We computed the median (instead of the average, as it was adopted in S14) of all $\Delta\nu_\ell$ as a better approximation to the observed large separation. No significant differences between $\Delta\nu_\ell$ and the median $\Delta\nu$ are found. Only a slightly larger dispersion was found for $\ell = 2$,

which is explained by the avoided-crossing phenomenon, not fully avoided by considering the median. In any case, such a dispersion, as happened in S14, was found to be statistically negligible. Therefore, in what remains of paper we will use only the average of the large separations $\langle\Delta\nu\rangle$.

3.2 Mean density corrected for the effect of rotation

In order to properly assess the impact of rotation on the $\Delta\nu$–$\bar{\rho}$ relation, it is important to consider the stellar deformation since it modifies the volume of the star. It is well known that the shape of a rotating star under the assumption of shellular rotation can be well approximated by a Roche potential model (equipotential surfaces). Nevertheless, a spheroid is a reasonable approximation up to almost 75 per cent of the break-up rotational velocity (see e.g. fig. 32 in Paxton et al. 2019). Since all our models are well below this value, we used the volume of a spheroid to compute the mean density. To that end, we needed to obtain the polar and equatorial radii from the parameters provided by CESTAM. So first, we need to understand what are those parameters.

Stellar structure quantities in CESTAM are defined as a mean variable over an isobar plus a perturbation term of the form (Marques et al. 2013)

$$f(p,\theta) = \bar{f}(p) + \tilde{f}_2(p)\, P_2(\cos\theta), \tag{2}$$

where $P_2(\cos\theta)$ is the second-order Legendre polynomial, p is the pressure, and θ is the colatitude. Moreover, r is defined as the mean radius of the isobar. This means that CESTAM's stellar radius indeed corresponds to the radius of a spherical symmetric model (hereafter, $R_{\rm SS}$) when $P_2(\cos\theta) = 0$, that is $\sin\theta^2 = 2/3$. Thus, following Pérez Hernández et al. (1999) and assuming that the polar radius, $R_{\rm p}$, barely changes with rotation for the same stellar mass, we can derive it as

$$R_{\rm p} = \frac{R_{\rm SS}}{1 + \frac{\Omega^2 R_{\rm SS}^3}{3GM}}, \tag{3}$$

where G is the gravitational constant, M is the stellar mass, and Ω is the angular rotational velocity.

To derive the equatorial radius, $R_{\rm e}$, we need to account for the stellar deformation. This is done using the fraction of critical rotation, $\omega = \Omega/\Omega_{\rm C}$. Here, $\Omega_{\rm C}$ is the critical angular rotation velocity, i.e. the velocity when the centrifugal and gravitational forces are balanced. At this point, $R_{\rm p} = 2/3R_{\rm e}$ (see e.g. Paxton et al. 2019). We can thus relate the critical rotational velocity with the polar radius as follows:

$$\Omega_{\rm C}^2 = \frac{8GM}{27R_{\rm p}^3}, \tag{4}$$

which allows us to relate both the equatorial and polar radii (see Paxton et al. 2019, for details) as

$$\frac{R_{\rm e}}{R_{\rm p}} = 1 + \frac{\omega^2}{2}. \tag{5}$$

We can now calculate the *correct* mean density of the models (as ellipsoids), from these radii as

$$V = \frac{3}{4\pi}\frac{M}{R_{\rm e}^2 R_{\rm p}}. \tag{6}$$

3.3 Discussion

Using CESTAM's output and computing the volume of a spherically symmetric model directly with the radius it provides can lead to noticeable differences (see Fig. 1). *Correct* mean densities are systematically lower (larger volumes), and it is noticeable that the $\Delta\nu$–$\bar{\rho}$ relation is tighter, i.e. the dispersion of points is reduced as compared with the spherically symmetric density.

Such effects modify slightly the fit of the overall behaviour of points in the $\Delta\nu$–$\bar{\rho}$ diagram:

$$\left(\frac{\bar{\rho}}{\rho_\odot}\right)_{\Omega} = 1.3867^{+0.0006}_{-0.0006}\left(\frac{<\Delta\nu>}{\Delta\nu_\odot}\right)^{1.8561^{+0.0004}_{-0.0004}} \tag{7}$$

$$\left(\frac{\bar{\rho}}{\rho_\odot}\right)_{\rm SS} = 1.0481^{+0.0005}_{-0.0005}\left(\frac{<\Delta\nu>}{\Delta\nu_\odot}\right)^{1.7894^{+0.0005}_{-0.0005}}, \tag{8}$$

where the subscript SS stands for the spherical symmetric case and Ω for the spheroid. Both fits have a Pearson correlation parameter above 0.97. The fact that fits are closer to empirical predictions (GH17) for deformed models gives us more confidence in our account for rotation in overall asteroseismic modelling. In addition, it illustrates the importance of properly considering the stellar shape when computing structure quantities of a deformed star. Hereafter, deformed models (non-spherical density models) are considered.

As in S14, we obtain a clear linear relation (in logarithmic scale) between the large separation and the mean density, although with significantly different fitting parameters. We found differences of about 20 per cent for the exponent and 70 per cent for the multiplicative factor with respect to S14's fit and around 10 per cent for the exponent and 50 per cent for the multiplicative factor compared to GH17's. In order to understand such differences, we studied the main *suspects*: metallicity, mass, and evolutionary stage distribution. In this work, an additional parameter comes into play: the stellar surface rotation.

The distribution of those parameters in the $\Delta\nu$–$\bar{\rho}$ diagram shows, as expected, a behaviour similar to what was found in S14 (Fig. 2). Metallicity is uniformly distributed with no specific trend. Rotational velocity shows a distribution that follows the evolution of the star with higher velocity for younger models (as expected) mainly located in the bunch of points around the middle of the panel (green/yellow dots). Regarding the central hydrogen fraction ($X_{\rm c}$), we found bands placed along the fit direction that reflects the evolutionary stage of the models, yet not explaining the major dispersion of points in the perpendicular direction. Finally, the only parameter of the four here analysed that does not depend on the stellar evolution is the mass, which shows gradient of bands perpendicular to the fit's direction. This is thus the main contributor to the width of the $\Delta\nu$–$\bar{\rho}$ diagram when all the models of the grid are displayed.

Because of their importance, we decided to go deeper into the analysis of both the $X_{\rm c}$ and M parameters combined. The bottom objective is to better understand the dependence of the fit with mass and Xc. For this purpose, we divided the model grid into 10 equal-mass range intervals on which we performed a linear regression to the $\Delta\nu$–$\bar{\rho}$ relation in logarithmic scale (see Fig. 3).

Notice that the highest mass range fit is the furthest away from the S14 and GH17 fits, whereas the lowest mass range is the closest to them. In between, there seems to be a *cluster* of models (generally late main sequence and subgiant branch) that determine the main weight of the fit, which move from the lower left to upper right parts of the panel.

In particular, for masses lower than 1.81 $M_\odot$, the differences in the exponent are of up to the 1 per cent with S14 and the 8 per cent with GH17. In the case of the multiplicative factor, these differences are up to the 55 per cent with S14 and the 33 per cent with GH17. However, when considering masses above 1.81 $M_\odot$ these differences become smaller with respect to GH17 but higher with respect to S14. Exponents were found to be lower by 12 per cent when compared

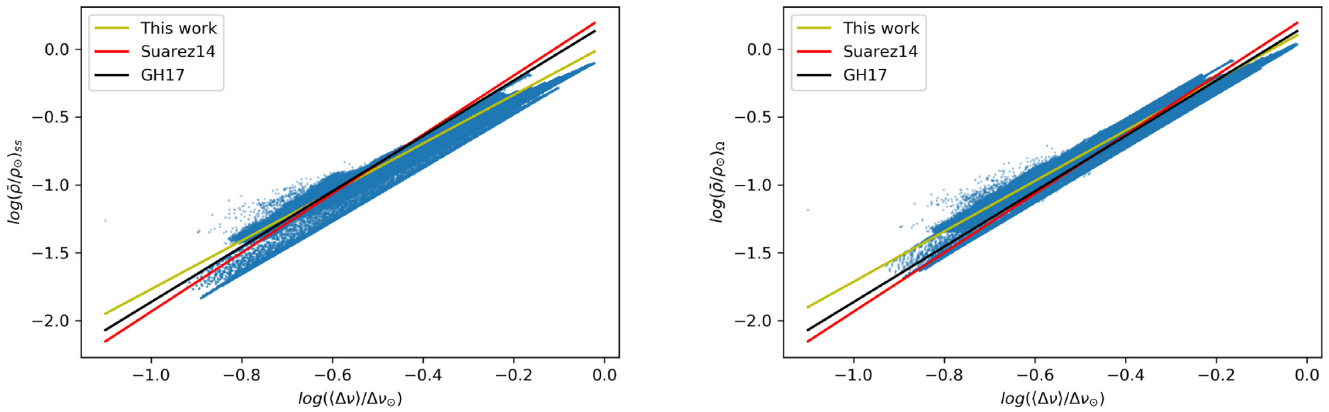

Figure 1. Mean density as a function of the average large separation, both in solar units and in logarithmic scale. The fit obtained in this work is represented, as also the linear fits obtained in previous works for comparison. The left-hand panel shows the relation for the spherical symmetric model and the right-hand panel for the spheroid (see the text for details).

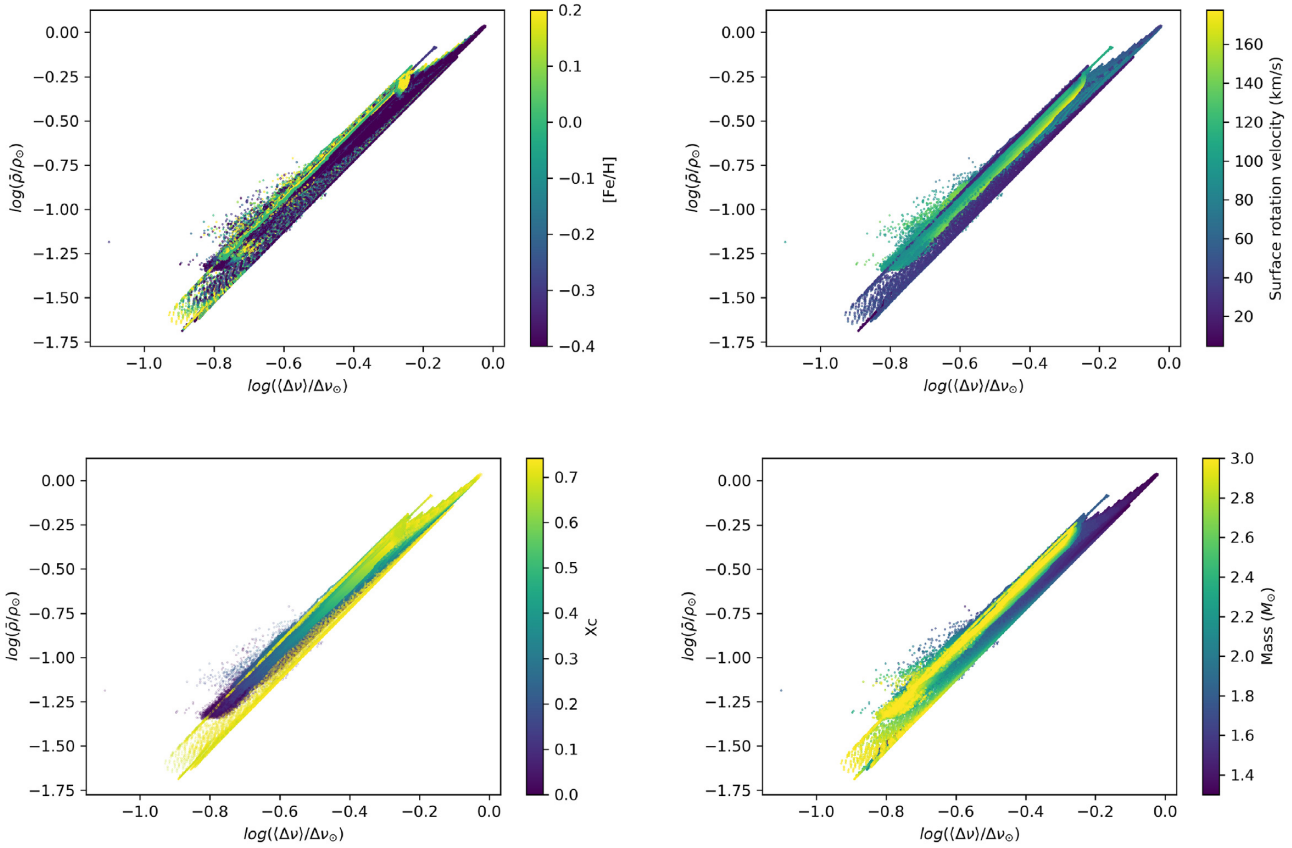

Figure 2. Mean density as a function of the large separation, both in logarithmic scale and normalized to the solar values. The different panels show the variation (as a colour scale) of the metallicity (top, left), the central hydrogen fraction (bottom, left), the surface rotation velocity at the equator (top, right), and mass (bottom, right).

with those given by S14, and lower by 6 per cent when compared with those by GH17. In the case of the multiplicative factor, they are lower by 38 and 18 per cent, respectively. The fact that the agreement in the multiplicative factor is always poorer was expected, since it is obtained via the independent term of the linear fit, and therefore it is a less precise value.

In addition, a subset of young models seems to populate the same region of the diagram whatever mass interval is considered, although with different sizes in the direction of the fit (yellow colour points in Fig. 3). We identify these as models in the ZAMS, or near the PMS close to the ZAMS. This range of models is well described by S14 and GH17 fits, and is compatible with the relations found with 2D pseudo-evolutionary models (Mirouh et al. 2019).

We then reduced the size of the mass *buckets* to the individual masses of the models in order determine the fit's actual dependence with mass. We applied thus the linear regression fit to all the models

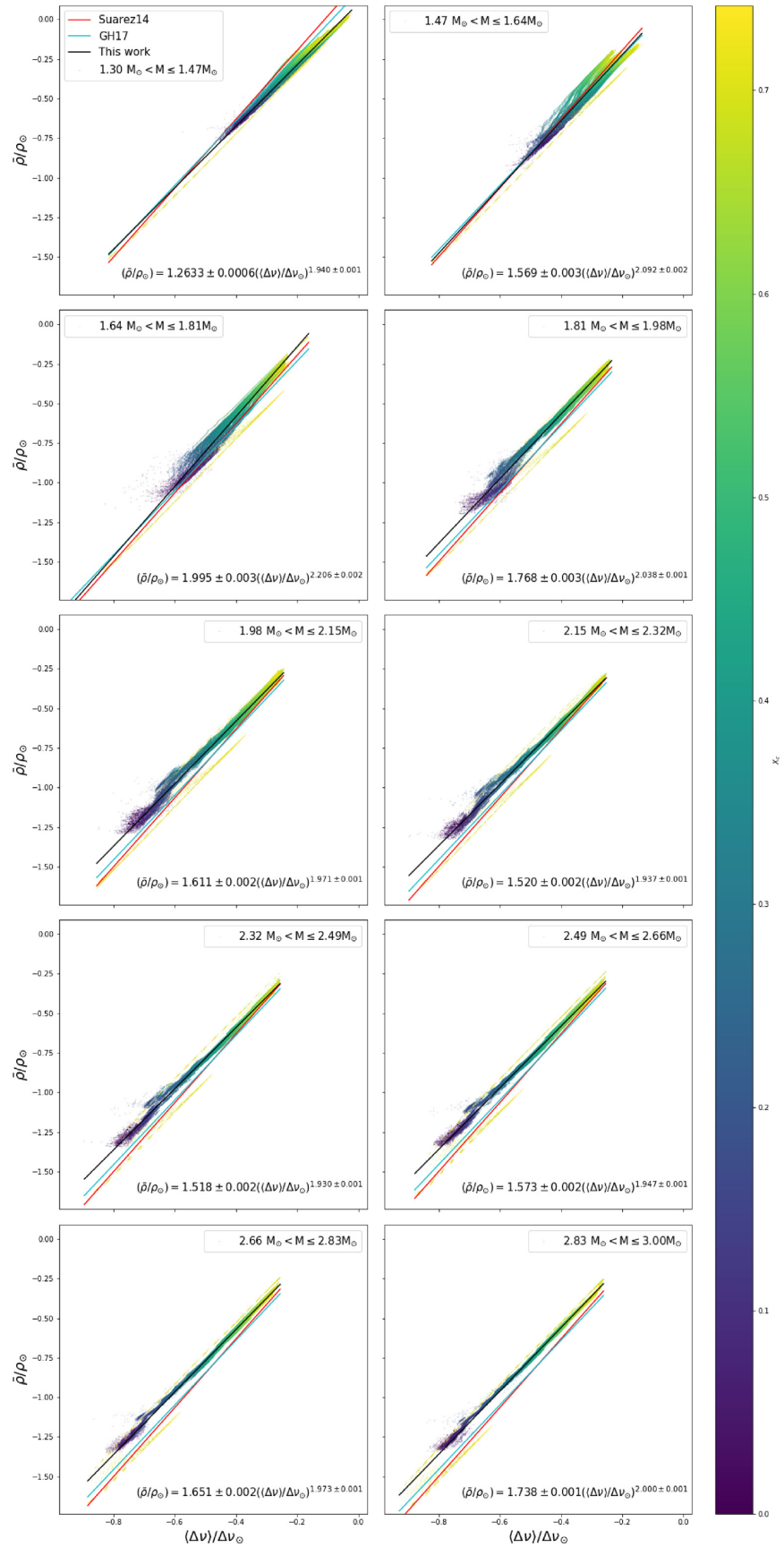

Figure 3. Mean density as a function of the large separation, both in logarithmic scale and normalized to the solar value, for the 10 mass intervals considered in this work. The central hydrogen mass fraction is represented in colour scale. For comparison, S14's and GH17's fits are also displayed.

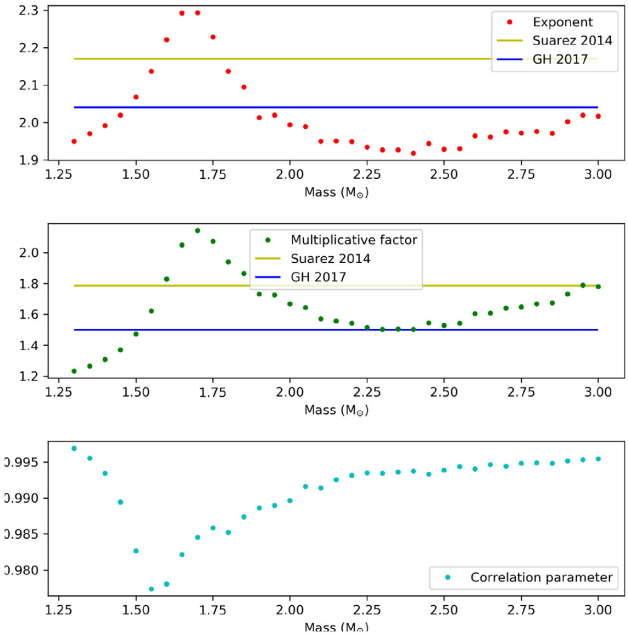

Figure 4. Upper panel: Value of the exponent of the fit as a function of mass. Results of previous works are represented for comparison. Middle panel: Value of the multiplicative factor of the fit as a function of mass. Results of previous works are represented for comparison. Lower panel: Correlation factor of each fit.

of each mass (Fig. 4). We found similar behaviour in both fitting parameters: There is an initial increase, reaching a peak at the same mass (about 1.70 $M_\odot$), and then decreasing until a plateau. In the case of the exponent, this plateau appears at a value close to that of the lowest mass (1.25 $M_\odot$) and corresponding to the minimum value of the exponent. Meanwhile, the multiplicative factor reaches a value that corresponds to the GH17's relation. The lowest value of the correlation parameter is around 0.970, meaning that all fits are very solid. The difference between the maximum and minimum values is about 20 per cent for the exponent and 75 per cent for the multiplicative factor.

It is worth noticing that the range of masses studied in S14 was 1.25–2.20 $M_\odot$. This means that the peak found in Fig. 4 takes a greater weight when fitting the models, and this would explain the greater values found in both fitting parameters of S14. On the other hand, in GH17 only three out of eleven stars had a mass below 1.81 $M_\odot$, meaning that most of the fitted stars fall in the plateau zone, which explains the significant resemblance with its value.

In order to get rid of the above dependence on the mass, and minimize the impact of the different number of models in different evolutionary stages, we calculated the mean values of the exponent and the multiplicative factor for all the masses:

$$\bar{\rho}/\rho_\odot = 1.6^{+0.5}_{-0.4}(\langle\Delta\nu\rangle/\Delta\nu_\odot)^{2.02^{+0.10}_{-0.10}}. \quad (9)$$

Then, the uncertainty in the exponent is simply the standard deviation and the multiplicative factor will go from the minimum to the maximum value, assuring the full coverage of the grid.

3.4 Application of a least-squares fit to calculate $\Delta\nu$

We investigated the impact of using the average of $\Delta\nu_\ell$ on the fit and thereby potentially on the conclusions. To do so, we compared our fits with those obtained using the generalized asymptotic formula (for

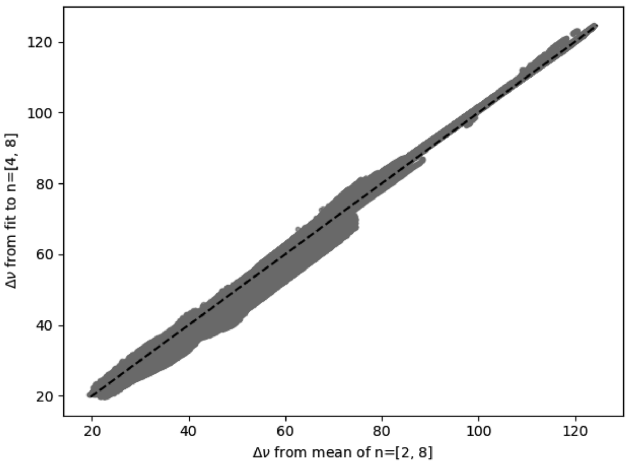

Figure 5. Comparison between $\Delta\nu$ obtained from our mean value and those obtained from fitting to $\nu = \Delta\nu(n + \varepsilon)$. See details in the text.

$n >> \ell$): $\nu = \Delta\nu(n + \varepsilon)$. Here, we cannot assume the asymptotic regime, so we use the phase ε that accounts for the deviation of that regime for frequencies of a given mode degree ℓ (see details in Bedding et al. 2020). To properly compare with that paper the fit is calculated considering only $\ell = 0$ frequencies with radial orders in the range $n = [4, 8]$. As can be seen in Fig. 5, both the average and linear square fits are compatible, with no significant difference that may modify the conclusions of this work. This result was somewhat expected since both n ranges overlap significantly.

Moreover, we also investigated the dependence of ε with other parameters that might influence it, like the impact of evolution (as suggested by Bedding et al. 2020). Interestingly, we found that the evolutionary state cannot be derived only from ε as shown in the right- and left-hand panels of Fig. 6. Notice the dependence with the mass and rotation rate in addition to stellar evolution, which implies that ε is not an optimum parameter to derive stellar ages. The discrepancies with Bedding et al.'s results might be due to the non-rotating models they used to calculate ε.

In any case, the results presented here are very preliminary and a more detailed study of the parameter is needed to derive any solid conclusion.

4 CHARACTERIZATION OF TWO δ SCT STARS: HD 174936 AND HD 174966

4.1 The data

HD 174936 and HD 174966 are δ Scuti stars (see Perryman et al. 1997; Lefèvre et al. 2009, respectively) observed by the *CoRoT* (Baglin et al. 2006) and *Gaia* (Perryman 2003; Gaia Collaboration 2016, 2018) satellites. *CoRoT* provided high-precision photometry during 27.2 d and *Gaia* obtained very precise parallaxes from which accurate and precise luminosities were derived.

HD 174636, whose spectral type is A2, was asteroseismologically characterized by García Hernández et al. (2009). They obtained a total of 422 significant oscillation frequencies. That made this star one of the two δ Scuti stars with the largest number of detected frequencies at that time, two orders of magnitude greater than from the ground. Using a Fourier transform technique, they found a frequency spacing that was identified as a low-order large separation.

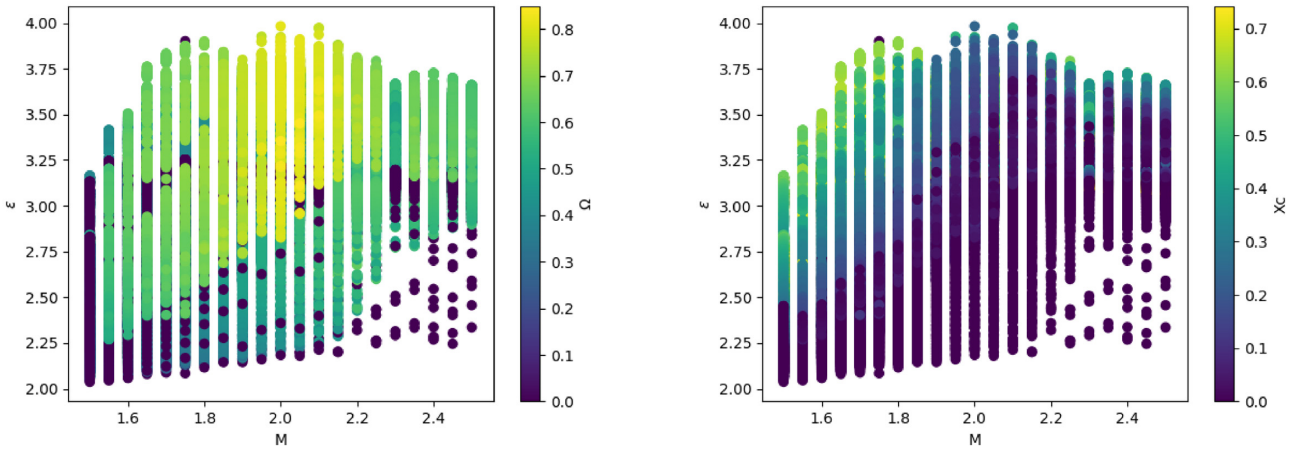

Figure 6. Left: ε as a function of mass. Colour code indicates the value of the rotation rate. Right: same as left, but colour code indicates the fraction of central hydrogen.

Similarly, HD 174966, with spectral type of A3, was studied for the preparation of the *CoRoT* target sample (Poretti et al. 2003). Later on, García Hernández et al. (2013) used the data obtained from the 27.2 d of uninterrupted *CoRoT* observation (initial run) to extract 185 significant peaks. As in previous works, the authors assumed the frequency spacing as a large separation (later confirmed theoretically and empirically by S14 and S15, respectively) to discriminate between representative models of the star.

However, these stars were characterized using stellar grids that did not consider rotation. Our grid can give an idea of the impact of rotation when constraining stellar parameters asteroseismologically. Moreover, luminosities from *Gaia* provide a new observable imposing additional constraints in the parameter space.

4.2 Characterization

The observables used for the characterization (see Table 2) were taken from GH09, GH13, and DR2 (Gaia Collaboration 2018). HD 174936 has only photometric parameters, whereas for HD 174966 there exist both photometric and spectroscopic measurements. Generally, the star's angle of inclination is unknown or has very large uncertainty. We decided thus not to include the rotational velocity as a constraint for model discrimination.

The procedure followed, analogues to that followed in GH13, is also applied to the spectroscopic parameters of HD 174966. First, we constrained models using the measured $T_{\rm eff}$, $\log g$, and metallicities from photometry within the 1σ uncertainties. Then, we used $\Delta\nu$ or *Gaia*'s luminosity as discriminant. The discrimination showed a tendency towards greater values in mass and luminosity compared to the non-rotating case (see Tables 3 and 4 for HD 1749436 and HD 174966, respectively). Deformation due to rotation allowed us to provide polar and equatorial radii (see Section 3.2). Some differences compared with García Hernández (2011) and GH13 are expected due to the inclusion of rotation in our models, although the expectations were to find lower masses and higher volumes, while preserving mean densities. However, we got systematically lower densities. We also find higher hydrogen abundances so less evolved stars.

These discrepancies might come from two different sources: first, the codes used in the computation of the equilibrium models. Each of them has different prescriptions in the physics and numerical schemes used to solve the structure and evolution equations. Secondly, the gravity darkening: Comparison between observations and modelling of rotating stars needs to consider that $T_{\rm eff}$ and $\log g$ are affected by the stellar deformation. Consequently, we did not take *Gaia*'s luminosity and $\Delta\nu$ simultaneously to discriminate models, since they do not show compatible restrictions (see Fig. 7).

None the less, our conclusions are still safe. Luminosity is more affected by gravity darkening than effective temperature (Paxton et al. 2019). We can thus consider the conservative uncertainties of the photometric parameters as a secure range for the real $T_{\rm eff}$ of our objects. We cannot consider $\log g$ either. On the contrary, $\Delta\nu$ has neither visibility nor deformation effects (because of the conservation of the $\bar{\rho}$–$\Delta\nu$ relation) and it is an alternative to $\log g$ (as shown by GH2017), so we can derive reliable parameters from these observables. Small uncertainties remain because of the unknown physics. Anyway, comparing *Gaia*'s luminosities with those coming from the constraints provided by $\Delta\nu$ might be used to get even more information about the stellar configuration, as we discuss in Section 4.3.

4.3 The role of the inclination angle *i*

As we discussed in Section 3.2, CESTAM's variables are split into a mean value over an isobar plus a perturbation. Thus, mean values of the variables correspond to $P_2(\cos\theta) = 0$, that is $\sin^2\theta = 2/3$ (Pérez Hernández et al. 1999). This means a colatitude $\theta \approx 54.7356^\circ$, as pointed out by Barceló Forteza, Roca Cortés & García (2018). Only the luminosity is not calculated in such a way. L is the integration of the flux all over the stellar surface, so it is the intrinsic stellar luminosity.

Then, the comparison between an observable independent of the inclination angle, such as $\Delta\nu$, and the observed luminosity will give some clue about i. In an HR diagram, a star with $i < 55^\circ$ would show a higher projected luminosity than the intrinsic one. And, on the contrary, when $i > 55^\circ$, the projected luminosity would be lower (see Paxton et al. 2019, for examples of both cases).

Our sample stars show both situations. HD 174936 shows a lower *Gaia* luminosity than $\Delta\nu$ so $i > 55^\circ$. That means a bounded rotational velocity between $v_{\rm rots} = [169.7, 207.2]$ km s^{-1}. On the other hand, HD 174966 is the opposite, with a higher *Gaia*'s luminosity and $i < 55^\circ$. GH13 estimated an inclination angle of $i = [45^\circ, 70^\circ]$, based on an LPVs (Line Profile Variations) analysis, with the most probable value at $i = 62.5^\circ$. With all these considerations,

Table 2. Observables used for the characterization of HD 174636 and HD 174966. The second row represents the photometric observables of HD 174966; meanwhile, the third represents the spectroscopic ones.

Star	$T_{\rm eff}$ (K)	log g	[Fe/H]	$\Delta\nu$ (μHz)	$L(L_\odot)$	$v_{\rm rots}$ (km s^{-1})
HD 174936	8000 ± 200^a	4.08 ± 0.20^a	-0.32 ± 0.20^a	52 ± 10^b	$[10.79, 11.15]^c$	$\geq 169.7^a$
HD174966	7637 ± 200^d	4.03 ± 0.20^d	-0.11 ± 0.20^d	65 ± 1^e	$[10.73, 10.93]^c$	$[135, 178]^e$
HD174966	7555 ± 50^e	4.21 ± 0.05^e	-0.08 ± 0.10^e	65 ± 1^e	$[10.73, 10.93]^c$	$[135, 178]^e$

References: [a]Charpinet et al. (2006), [b]GH09, [c]Gaia Collaboration (2018), [d]Solano et al. (2005), and [e]GH13.

Table 3. Characterization of HD 174936 taking 1σ uncertainties in each observable. The second column shows the physical characterization obtained using the photometric measurements. The third column represents the values obtained when applying the large separation criteria to the photometric box subset of models. The fourth column represents the values obtained when using $T_{\rm eff}$ and *Gaia*'s L.

Parameter	Photometry	Photometry + $\Delta\nu$	Photometry + $L_{\rm Gaia}$
M ($M_\odot$)	[1.70, 2.45]	[1.85, 2.20]	[1.80, 1.95]
$R_{\rm p}$ ($R_\odot$)	[1.53, 2.89]	[1.96, 2.20]	[1.60, 1.80]
Re ($R_\odot$)	[1.60, 3.41]	[2.13, 2.61]	[1.75, 2.00]
L ($L_\odot$)	[8.54, 35.56]	[14.03, 20.79]	[10.87, 11.07]
$T_{\rm eff}$ (K)	[7800.00, 8199.98]	[7800.02, 8199.81]	[7800.07, 8198.43]
log$g$	[3.88, 4.28]	[4.05, 4.12]	[4.17, 4.27]
Xc	[0.22, 0.74]	[0.40, 0.53]	[0.53, 0.74]
$\bar{\rho_\Omega}$ (g cm^{-3})	[0.104, 0.599]	[0.211, 0.292]	[0.369, 0.542]
[Fe/H]	[−0.4, −0.2]	[−0.4, −0.2]	[−0.4, −0.2]

Table 4. Characterization of HD 174966 taken 1σ uncertainties in the considered observables. The second, third, and fourth columns represent the same constraints as in Table 3 but for HD 174966. The fifth column shows the limits of the physical parameters when using the spectroscopic measurements and the sixth one when also considering $\Delta\nu$.

Parameter	Photometry	Phot. + $\Delta\nu$	Phot. + $L_{\rm Gaia}$	Spec.	Spec. + $\Delta\nu$
M ($M_\odot$)	[1.70, 2.30]	[1.75, 1.85]	[1.85, 1.85]	[1.70, 1.80]	[1.75, 1.80]
$R_{\rm p}$ ($R_\odot$)	[1.63, 2.95]	[1.69, 1.76]	[1.85, 1.90]	[1.58, 1.82]	[1.70,1.75]
$R_{\rm e}$ ($R_\odot$)	[1.73, 3.52]	[1.82, 1.99]	[2.02, 2.15]	[1.67,2.02]	[1.82, 1.95]
L ($L_\odot$)	[7.58, 30.73]	[8.18, 11.02]	[10.74, 10.92]	[7.34, 10.23]	[8.74, 9.33]
$T_{\rm eff}$ (K)	[7437.04, 7836.98]	[7437.92, 7836.98]	[7506.81, 7621.67]	[7505.03, 7604.95]	[7505.16, 7604.32]
log$g$	[3.83, 4.23]	[4.19, 4.22]	[4.12, 4.16]	[4.16, 4.26]	[4.19, 4.21]
Xc	[0.20, 0.72]	[0.56, 0.61]	[0.50, 0.54]	[0.53, 0.72]	[0.56, 0.60]
$\bar{\rho_\Omega}$ (g cm^{-3})	[0.090, 0.489]	[0.375, 0.446]	[0.296, 0.347]	[0.345, 0.543]	[0.381, 0.438]
[Fe/H]	[−0.1, 0.0]	[−0.1, 0.0]	[0.0, 0.0]	[−0.1, 0.0]	[−0.1, 0.0]

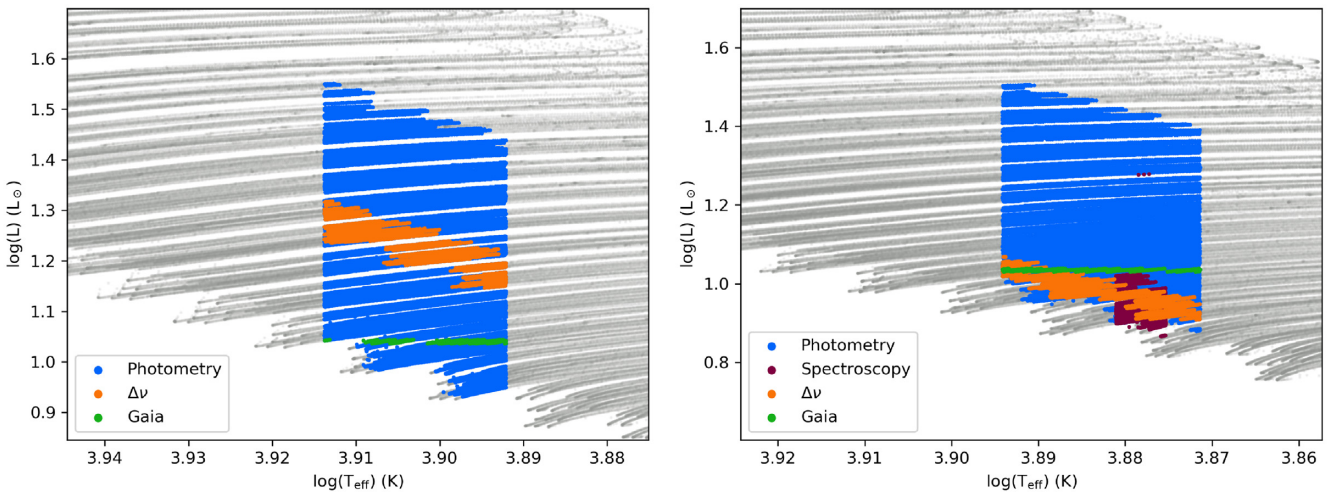

Figure 7. HR diagrams showing error boxes obtained for HD 174936 (left) and HD 174966 (right). Sources of uncertainty are depicted in different colours over the evolutionary tracks (grey).

the rotational velocity of this star seems to be in the range of $v_{\rm rots} = [135, 153]$ km s^{-1}, corresponding to $i = [45°, 55°]$. In any case, this angle must not be very far from 55°, since *Gaia*'s and $\Delta\nu$ luminosities slightly overlap for the photometric $T_{\rm eff}$.

A more detailed analysis could give a more precise value of i. This is not the scope of this research but it will be investigated in a forthcoming work.

5 CONCLUSIONS

We have conducted a study of the impact of rotation on the relation between the predicted large separation and mean density in the low-order regime. This work updates the study performed by Suárez et al. (2014) with non-rotating models. Here we have updated that work by assessing in detail the effect of the moderate rotation on the $\Delta\nu$–$\bar{\rho}$ relation. We have computed a grid of rotating asteroseismic models representative of intermediate-mass stars.

We have first confirmed the consistency of our modelling when computing the mean density of the models on a deformed surface (ellipsoid). The fits obtained are closer to the empirical ones than those obtained with $\bar{\rho}$ from spherically symmetric models. Although differences do not change the overall behaviour, they become important when those fits are employed to characterize individual stars. For example, mean densities are clearly different when not considering a spheroid volume.

The linear relation for the rotating models was found in line with the previous predictions (S14), as well as with empirical results (García Hernández et al. 2015, 2017). Like in those works, we have found a dispersion in this relation, explained mainly by the stellar mass. The detailed comparison by mass ranges (buckets) yields a systematic variation of the coefficients all along the whole mass range. The majority of the individual fits remain within those found by the aforementioned works, favouring the matching for highest masses. Additionally, most of the individual fits for masses larger than 1.8 $M_\odot$ are closer to the empirical one (GH17) except for the very highest masses close to 3 $M_\odot$, making it even more reliable for δ Scuti stars.

We carried out an extra test to characterize the parameter ε from a fit to the frequencies following the classical asymptotic relation: $\nu = \Delta\nu(n + \varepsilon)$, also used in Bedding et al. (2020). In contrast to their findings, we could not establish a clear relation between this parameter and the evolutionary state of the model. This is maybe due to the dependence on rotation but additional work must be done in this sense to clarify these conclusions.

Following the methodology used in García Hernández et al. (2013), we applied the new fit obtained for rotating stars to constrain global parameters of the δ Scuti stars HD 174936 and HD 174966, with the objective of comparing the results with previous works in which rotation was not taken into account. The models constrained this way were then confronted with the observed temperatures and surface gravities obtained from spectroscopy and photometry, including luminosities from *Gaia*'s DR2 data. For both stars, we predict systematic lower densities as well as higher hydrogen abundances than those for the non-rotating case. This would imply that both stars are less evolved than has been characterized in GH09 and GH13.

Additionally, the discrepancies found in the luminosities derived from $\Delta\nu$ and those observed by *Gaia* allow us to discuss the effects of gravity darkening in our study. In particular, for HD 174936, the analysis of limb darkening allowed us to determine a lower bound for the angle of inclination ($i > 55$ deg), and thereby the surface rotational velocity is bounded to $v_{\rm rots} = [169, 207]$ km s^{-1}. On the other hand, for HD 174966 we found an upper bound for the angle of inclination ($i < 55$ deg), which allowed us to constrain the surface rotational velocity to $v_{\rm rots} = [135, 153]$ km s^{-1}. This implies an angle of inclination of $i = [45, 55]$ deg, which is a smaller value than GH13's predictions (although still compatible with that work's results within the 1σ uncertainty in i).

We have thus (1) confirmed the robustness and reliability of the empirical $\Delta\nu$–$\bar{\rho}$ relation given by GH17, providing new limits to the relation (equation 9) that encompass any possible dependence on mass, and (2) found a reliable methodology using 1D-evolutionary rotating models and perturbative theory for characterizing moderately fast rotating stars. This methodology allows us to constrain the angle of inclination of the star and hence the actual surface rotational velocity. Yet this constraint is still small, and additional information on i is required. We plan to deepen on this by studying objects for which both high-resolution spectroscopy and interferometry measurements are available (e.g. the stars Altair or Rasalhague).

Furthermore, we want to investigate how our method can be used in the construction of 2D rotating models, e.g. with the ESTER code, as it may provide sufficiently accurate constraints to get the *seed*-1D model for the 2D computations.

ACKNOWLEDGEMENTS

The authors want to strongly thank Dr. Daniel R. Reese for his very professional and useful report that helped us to significantly improve the paper.

The authors acknowledge funding support from Spanish public funds (including FEDER funds) for research under projects ESP2017-87676-C5-2-R, ESP2017-87676-C5-5-R, and PID2019-107061GB-C64. Julio E. Rodríguez-Martín also acknowledges financial support from the State Agency for Research of the Spanish Ministerio de Ciencia, Innovación y Universidades through the 'Center of Excellence Severo Ochoa' award to the Instituto de Astrofísica de Andalucía-Consejo Superior de Investigaciones Científicas (SEV-2017-0709). Antonio García Hernández also acknowledges support from 'Fondo Europeo de Desarrollo Regional/Junta de Andalucía-Consejería de Economía y Conocimiento' under project E-FQM-041-UGR18 by Universidad de Granada. Juan Carlos Suárez also acknowledges support from project RYC-2012-09913 under the 'Ramón y Cajal' programme of the Spanish Ministry of Science and Education. This work has made use of data from the European Space Agency (ESA) mission *Gaia* (https://www.cosmos.esa.int/gaia), processed by the *Gaia* Data Processing and Analysis Consortium (DPAC; https://www.cosmos.esa.int/web/gaia/dpac/consortium). Funding for the DPAC has been provided by national institutions, in particular the institutions participating in the *Gaia* Multilateral Agreement.

DATA AVAILABILITY

The data underlying this article will be shared on reasonable request to the corresponding author.

REFERENCES

Aerts C., Christensen-Dalsgaard J., Kurtz D. W., 2010, Asteroseismology. Springer, the Netherlands

Baglin A., Michel E., Auvergne M., 2006, in Fridlund M., Baglin A., Lochard J., Conroy L., eds, ESA SP-1306: Stellar Seismology and Planet Finding. ESA, Noordwijk, p. 39

Barceló Forteza S., Roca Cortés T., García R. A., 2018, A&A, 614, A46

Bedding T. R. et al., 2020, Nature, 581, 147

Charpinet S., Cuvilo J., Platzer J., Deleuil M., Catala C., Baglin A., 2006, in Fridlund M., Baglin A., Lochard J., Conroy L., eds, ESA SP-1306: The CoRoT Mission Pre-Launch Status – Stellar Seismology and Planet Finding. ESA, Noordwijk, p. 353
Dupret M. A., Grigahcène A., Garrido R., Gabriel M., Scuflaire R., 2005, A&A, 435, 927
Gaia Collaboration, 2016, A&A, 595, A1
Gaia Collaboration, 2018, A&A, 616, A1
García Hernández A., 2011, PhD thesis, Instituto de Astrofísica de Andalucía (CSIC)
García Hernández A. et al., 2009, A&A, 506, 79
García Hernández A. et al., 2013, A&A, 559, A63
García Hernández A., Martín-Ruiz S., Monteiro M. J. P. F. G., Suárez J. C., Reese D. R., Pascual-Granado J., Garrido R., 2015, ApJ, 811, L29
García Hernández A. et al., 2017, MNRAS, 471, L140
Gilliland R. L. et al., 2010, PASP, 122, 131
Lebreton Y. et al., 2008, Ap&SS, 316, 1
Lefèvre L. et al., 2009, Commun. Asteroseismol., 158, 189
Marques J. P. et al., 2013, A&A, 549, A74
Mathis S., Zahn J.-P., 2004, A&A, 425, 229
Matthews J. M., 2007, Commun. Asteroseismol., 150, 333
Mirouh G. M., Angelou G. C., Reese D. R., Costa G., 2019, MNRAS, 483, L28
Moya A., Garrido R., 2008, Ap&SS, 316, 129
Moya A., Suárez J. C., Hernández A. G., Mendoza M. A., 2017, MNRAS, 471, 491
Murphy S. J., Hey D., Van Reeth T., Bedding T. R., 2019, MNRAS, 485, 2380
Ouazzani R.-M., Roxburgh I. W., Dupret M.-A., 2015, A&A, 579, A116
Paxton B. et al., 2019, APJS, 243, 10
Pérez Hernández F., Claret A., Hernández M. M., Michel E., 1999, A&A, 346, 586
Perryman M. A. C., 2003, Gaia Spectrosc. Sci. Technol., 298, 3
Perryman M. A. C. et al., 1997, A&A, 500, 501
Poretti E. et al., 2003, A&A, 406, 203
Reese D., Lignières F., Rieutord M., 2008, A&A, 481, 449
Reese D. R., Lignières F., Ballot J., Dupret M. A., Barban C., Van 'T Veer-Menneret C., Macgregor K. B., 2017, A&A, 601, A130
Ricker G. R. et al., 2009, Am. Astron. Soc. Meeting Abstr., 214, 306.05
Rodríguez E., Breger M., 2001, A&A, 366, 178
Royer F., Zorec J., Gómez A. E., 2007, A&A, 463, 671
Solano E. et al., 2005, AJ, 129, 547
Suárez J. C., Goupil M. J., 2008, Ap&SS, 316, 155
Suárez J. C., Goupil M. J., Morel P., 2006, A&A, 449, 673
Suárez J. C., García Hernández A., Moya A., Rodrigo C., Solano E., Garrido R., Rodón J. R., 2014, A&A, 563, A7
Uytterhoeven K. et al., 2011, A&A, 534, A125
Xiong D. R., Deng L., Zhang C., Wang K., 2016, MNRAS, 457, 3163
Zahn J. P., 1992, A&A, 265, 115

This paper has been typeset from a TEX/LATEX file prepared by the author.